



Pd and Pd-Cu supported on different carbon materials and immobilized as flow-through catalytic membranes for the chemical reduction of NO_3^- , NO_2^- and BrO_3^- in drinking water treatment

Adrián Marí^a, José Alberto Baeza^{a,*}, Marta Pedrosa^{b,c}, O. Salomé G.P. Soares^{b,c}, Luisa Calvo^a, Miguel Ángel Gilarranz^a, Adrián M.T. Silva^{b,c}, M. Fernando R. Pereira^{b,c}

^a Departamento de Ingeniería Química, Universidad Autónoma de Madrid, C/Francisco Tomás y Valiente 7, Madrid 28049, Spain

^b LSRE-LCM - Laboratory of Separation and Reaction Engineering - Laboratory of Catalysis and Materials, Faculty of Engineering, University of Porto, Rua Dr. Roberto Frias, Porto 4200-465, Portugal

^c ALiCE - Associated Laboratory in Chemical Engineering, Faculty of Engineering, University of Porto, Rua Dr. Roberto Frias, Porto 4200-465, Portugal

ARTICLE INFO

Stefanos Giannakis

Keywords:

Oxoanion reduction
Catalytic membrane
Flow-through configuration
Pd-Cu catalysts
Carbon

ABSTRACT

Powdered catalysts are commonly used in lab-scale tests for the catalytic reduction of oxoanions in drinking water, but their powder nature limits their application at full scale. In this work, Pd and Pd-Cu catalysts (5% wt.) supported on carbon materials with different structural properties, in powder form, were used to prepare catalytic membranes that were tested in a reactor with flow-through configuration (FTCMR) to study their performance in the reduction of NO_3^- , NO_2^- and BrO_3^- . Pd catalytic membranes showed high activity in the reduction of NO_2^- , being the selectivity to NH_4^+ lower than 2% at 80% NO_2^- conversion in all cases. In BrO_3^- reduction, they exhibited a wide range of conversions being the catalyst supported on materials with high conductivity the most active ones, which may be ascribed to the charge distribution at the metal-carbon interface. NO_3^- reduction using Pd-Cu catalytic membranes showed that catalysts supported on materials with small nanoparticle size and low electrical conductivity exhibited higher selectivity to NH_4^+ . FTCMR led to a good control of H_2 transfer and availability in the active sites, facilitating the tuning of H_2 availability conditions to preserve the activity, while maintaining/diminishing selectivity to NH_4^+ . In simultaneous oxoanions reduction tests, NO_3^- reduction was inhibited by Br species, probably by affection of the Pd-Cu redox cycle. This fact could be crucial to the future development of drinking water treatment processes, as conditions the order of the disinfection and NO_3^- reduction steps.

1. Introduction

With the rapid development of the economy and society, rivers, lakes, and groundwater in many areas have suffered different degrees of pollution, and the water quality has been degraded severely [1]. Thus, oxoanions such as NO_3^- , NO_2^- and BrO_3^- have caught increased attention since, in addition to appearing in water sources, they are also present in treated drinking water [2]. NO_3^- pollution derives from a wide range of pathways, such as the excessive use of fertilizers in intensive agriculture, leaking of septic tanks and waste disposal in breeding farms [3]. The EU regulation (Directive 2020/2184) [4] sets maximum concentrations of 50 and 0.1 mg/L for NO_3^- and NO_2^- , respectively, in drinking water and the World Health Organization (WHO) recommends a limit of 10 mg/L

N- NO_3^- (44 mg/L NO_3^-) in drinking water [5]. BrO_3^- is a disinfection by-product from the ozonation or advanced oxidation of water containing bromide. Currently, the European Union and the U.S. Environmental Protection Agency (EPA) have set a maximum level of 10 $\mu\text{g/L}$ (0.078 $\mu\text{mol/L}$) for BrO_3^- in drinking water. There are different techniques for NO_3^- , NO_2^- and BrO_3^- removal, such as reverse osmosis, electrodialysis, ion exchange, among others. Nevertheless, these techniques present some limitations such as high costs and the necessary post-treatment steps.

Catalytic reduction is being investigated in the last decades as a potential solution since it is addressed to convert NO_3^- into harmless gaseous N_2 using a reducing agent such as H_2 , without generating any secondary waste. However, the formation of NO_2^- and/or NH_4^+ has been

* Corresponding author.

E-mail address: josealberto.baeza@uam.es (J.A. Baeza).

<https://doi.org/10.1016/j.jece.2023.109772>

Received 15 November 2022; Received in revised form 14 February 2023; Accepted 22 March 2023

Available online 25 March 2023

2213-3437/© 2023 The Author(s). Published by Elsevier Ltd. This is an open access article under the CC BY-NC-ND license (<http://creativecommons.org/licenses/by-nc-nd/4.0/>).

so far its main limitation avoiding practical use. Effective NO_3^- reduction takes place using bimetallic catalysts consisting of a noble metal (Pd, Pt, Rh...) and a metal promoter (Cu, Sn, Ni...), whereas NO_2^- and BrO_3^- reduction can occur with a monometallic catalyst, commonly Pd. This metallic phase is commonly supported on different materials such as carbon, alumina or other metal oxides, among others.

The use of catalytic membranes represents a very broad field of research, including fuel cells [6] and photocatalysis [7]. However, references based on oxoanion reduction are scarce. Membrane fabrication methods are also diverse. Among them, membrane preparation by vacuum filtration stands out as a fast and simple method. This process is driven by the negative pressure on one side of the filter medium, leading to solid-liquid separation and catalyst deposition on a commercial support [8]. In addition, the use of a polymeric membrane support, leading to a multilayer membrane, avoids the use of binders, which would hinder access to the active centers. Likewise, the polymeric membrane support prevents contamination of the treated water by nanomaterials and catalysts. There are numerous reports of the use of membranes formed by vacuum filtration in both, oxidation [9,10] and reduction [11] of organic compounds. In this work, procedures for the fabrication of the membranes have been based on previous developments made by the authors [12,13].

Catalytic membrane reactors (CMR) have been developed as an alternative to conventional reactors, such as batch or fixed beds. Flow-through catalytic membranes are a type of unselective permeability catalytic membranes that work in dead-end mode, forcing the flow to move across the porosity of the membrane and, thus, favouring an intense contact between reactants and catalytic sites with a short, controlled contact time, thus minimizing or avoiding membrane internal diffusion limitations [14]. Traditionally, this sort of catalytic membranes has been used in processes where high catalytic activity with a short residence time can be achieved, or in processes where high selectivity to desired products can be obtained by taking advantage of the narrow reactant distribution across the membrane. Regarding the latter, partial hydrogenation reactions are considered good candidates for the application of flow-through catalytic membranes, as undesired side hydrogenation reactions are a common drawback [15]. Hydrogenation in aqueous medium is usually limited by H_2 availability due to its low solubility, leading to low reaction rates when a single-pass mode through the membrane is used. Thus, a liquid-recycling mode is applied to enhance the performance [14]. The liquid flow circulates from a H_2 saturation tank connected in loop to the flow-through catalytic membrane reactor (FTCMR) that acts as a differential reactor, as shown in Scheme 1.

In contrast to three-phase catalytic reactors with single-pass mode, the FTCMR system takes advantage of the low H_2 concentration at the catalyst surface and low concentration gradient across the membrane, limiting undesired side hydrogenation reactions [15]. Some of the advantages of the FTCMRs are the better liquid-solid contact, avoiding

gas-solid contact, and reducing differences between textural properties in terms of wettability compared to slurry reactors. Moreover, FTCMRs can be useful tools to test the influence of H_2 availability on catalyst performance as residence time is timely controlled.

To the best of our knowledge, reports on the use of FTCMRs are scarce, especially for the application to NO_3^- , NO_2^- and BrO_3^- reduction in water [16,17]. Studies on the catalytic reduction of oxoanions, assessing the performance of different powder-based catalysts on slurry reactors are common in the literature, but their application to real drinking water treatment is compromised because of the powder nature of the catalysts. The FTCMR could represent a feasible alternative to the application of powder-based catalysts with good performance in slurry reactors, but that can hardly be used in fixed-bed reactors, due to the small particle size that could provoke drastic pressure drops in the system or even clogging the filters supporting the catalytic bed. The FTCMR can achieve equivalent conversion with similar and even lower selectivity to NH_4^+ than a slurry reactor while operating with lower H_2 flow [18], although direct comparison is not possible due to differences in configuration and operation conditions. Additional features of FTCMR include immobilization of catalyst facilitating scaling-up, whereas the industrial application of powder catalysts in slurry reactors is very limited.

Additional features of FTCMR include immobilization of catalyst facilitating scaling-up, whereas the industrial application of powder catalysts in slurry reactors is very limited.

In this work, different Pd-Cu catalysts supported on carbon materials with different structural and physicochemical properties have been studied in a membrane reactor with FTCMR configuration for enhanced control of H_2 availability at the catalyst for separate and simultaneous NO_3^- , NO_2^- and BrO_3^- reduction. The influence of Br species in catalyst behavior has also been explored.

2. Experimental

2.1. Materials

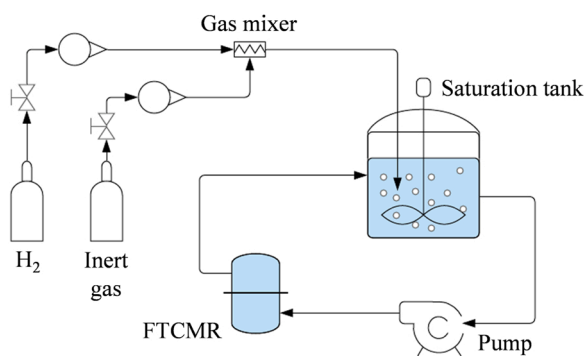
$\text{CuCl}_2 \cdot 2\text{H}_2\text{O}$ (99.9%), PdCl_2 (99%), NaBrO_3 (99%), NaBr (99%), graphite (G), graphitized carbon nanofibers (CNF) and 2,6-pyridinedicarboxylic acid (99.5%) were supplied by Sigma-Aldrich. HNO_3 (65%), NaNO_3 (99%), NaNO_2 (98%), NH_4Cl (99.5%), Na_2CO_3 (99%), and NaHCO_3 (99.5%) were provided by Panreac. Activated carbon (AC), reduced graphene oxide (rGO) and ENSACO250G carbon black (ENS250) were purchased from Norit, Graphenea and Timcal, respectively. H_2 and CO_2 were supplied by Nippon gases.

2.2. Preparation and characterization of catalytic materials

Pd/C catalysts (5 wt%; C = CNF, rGO, AC or ENS250) were prepared by wet impregnation. A PdCl_2 solution in 0.1 M HCl was introduced in a rotary-evaporator along with the support, being mixed until complete dryness at 70 °C, 150 mbar and 200 rpm. Then, the catalysts were dried overnight at 60 °C, calcined at 200 °C for 2 h and reduced with H_2 at 25 cm^3 STP/min flow rate for 2 h at 200 °C.

Pd-Cu/C catalysts (5 wt%; C = G, CNF, rGO, AC or ENS250) with a Pd:Cu weight ratio of 2:1 were prepared by successive wet impregnation where a PdCl_2 solution in 0.1 M HCl was mixed with the corresponding support in a rotary-evaporator at 70 °C, 150 mbar and 200 rpm. Then, this step was repeated using a $\text{CuCl}_2 \cdot 2\text{H}_2\text{O}$ solution. Finally, the catalysts were left overnight at 60 °C, calcined at 200 °C for 2 h and reduced at 200 °C for 2 h at 25 cm^3 STP/min of H_2 flow rate.

The catalytic membranes were prepared by vacuum filtration of a known volume of catalyst suspension with polypropylene filters (0.22 μm), using a Kitasato and a Büchner funnel coupled to a vacuum pump. The catalysts were suspended in ultrapure water and ultrasonicated for 1 h before membrane preparation. The mass of catalyst (Pd/C or Pd-Cu/C) in the membrane was 20 and 60 mg for membranes of 16 and 30 mm in diameter, respectively, resulting in a mass load



Scheme 1. Flow-through catalytic membrane reactor (FTCMR) with liquid-recycling mode.

between 8.5 and 10 mg/cm². The membranes stability was checked after the reduction tests. They remained homogeneous, without detachments nor agglomerations after the essays, as shown in the [Supplementary Material \(Fig. S1\)](#).

The Pd/C catalysts were characterized by TEM, using a JEOL JEM 3000 F equipment, and H₂ chemisorption to assess the dispersion of the metal phase of the catalysts. These experiments were performed in an Altamira AMI-200 apparatus. Pulses of H₂ were injected in a carrier gas (25 cm³ STP/min of Ar) and this mixture was flowed through the samples until metal saturation. The adsorbed hydrogen quantity was measured using a thermal conductivity detector (TCD). The Pd-Cu/C catalysts were characterized by TEM and EDX using same equipment. XPS characterization (K-Alpha Thermo Scientific equipped with an AlK α X-ray excitation source, 1486.68 eV) was also carried out to obtain the extent of Pd and Cu oxidation state in Pd-Cu/C fresh and used catalysts. XPSPEAK v4.1 software was used to deconvolute the signals and calculate zerovalent and electro-deficient metal species.

Characterization of the supports by adsorption-desorption N₂ isotherms at 77 K and electrical conductivity, along with previous Pd-Cu/rGO and Pd-Cu/CNF catalysts characterization by TEM analysis was reported in a previous work [18] and are summarized in [Tables S1-S3](#).

2.3. Experimental set-up and tests

The set-up consisted of a stirred round-bottomed glass, used as H₂ and CO₂ saturation tank, connected to a peristaltic pump that circulates liquid to the FTCMR. The outlet of the FTCMR is connected to the saturation tank to achieve reaction medium recirculation. The FTCMRs were home-made designed (40 mm × 34 mm × 34 mm) and made of methacrylate, as shown in [Fig. 1](#). FTCMRs were made to allocate 16 mm- and 30 mm-diameter membranes.

The experimental runs were carried out using 60 mL of reaction volume at ambient temperature and pressure. In a typical test, 58.8 mL of water was saturated under a 100 cm³ STP/min of a mixture of H₂ and CO₂ (1:1 v/v) flow rate and recirculated through the FTCMR for 30 min. In some experiments, H₂ flow rate in the saturation tank was varied between 50 and 10 cm³ STP/min to explore the effect of H₂ availability in the system, whereas the CO₂ flow rate was maintained at 50 cm³ STP/min. pH values remained between 4.5 and 5 during the reaction runs. The surface velocity in the FTCMR was 0.5 cm/min. After stabilization of the FTCMR system, 1.2 mL of 1500 mg/L pollutant solution was injected into the saturation tank to achieve a starting pollutant concentration of 30 mg/L. BrO₃⁻, NO₂⁻ and NO₃⁻ were tested as pollutants. The replicability of the assays was verified in selected experiments. The calculated error did not exceed ±8%.

Samples were periodically collected from the system for 4 h. The samples were characterized by ionic liquid chromatography (Metrohm 882 Compact IC plus anion and cation) with a Metrosep C6 column and a mixture of 1.7 mM of HNO₃ and 1.7 mM of 2,6-pyridinedicarboxylic acid eluent (0.9 mL/min) for cation separation. For anion separation, a Metrosep A Supp 5 column and a mixture of 3.2 mM Na₂CO₃ and 1 mM NaHCO₃ (0.7 mL/min) were used.

Pollutant conversion was calculated according to [Eq. \(1\)](#) (given for NO₃⁻ as example). Selectivity to NO₂⁻ and NH₄⁺ were calculated according to [Eqs. 2 and 3](#) (given for NO₃⁻ as example):

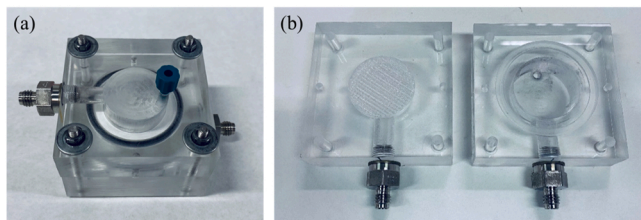


Fig. 1. (a) Assembled and (b) unassembled FTCMR.

$$X_{NO_3^-}(\%) = \frac{n_{NO_3^-,t=0} - n_{NO_3^-,t}}{n_{NO_3^-,t=0}} \cdot 100 \quad (1)$$

$$S_{NO_2^-}(\%) = \frac{n_{NO_2^-,t}}{n_{NO_3^-,t=0} - n_{NO_3^-,t}} \cdot 100 \quad (2)$$

$$S_{NH_4^+}(\%) = \frac{n_{NH_4^+,t}}{n_{NO_3^-,t=0} - n_{NO_3^-,t}} \cdot 100 \quad (3)$$

where $n_{i,t=0}$ is the initial amount of compound i (mol) and $n_{i,t}$ is the amount of compound i (mol) at time t (min).

3. Results and discussion

3.1. Support and catalysts characterization

Support characterization can be found elsewhere [18], but results related to textural properties and conductivity are summarized in [Supplementary Material \(Tables S1 and S2\)](#).

[Fig. 2](#) shows representative TEM micrographs of Pd/C catalysts, nanoparticle size distributions, along with mean sizes and standard deviations. All the catalysts presented Pd nanoparticles in a range from 1.3 to 5.0 nm. Pd/CNF also showed a pronounced tail beyond 12 nm, compared to other catalysts. TEM characterization of bimetallic Pd-Cu catalysts can be found elsewhere [18], but for clarity, nanoparticles mean size and standard deviations are summarized in [Supplementary Material \(Table S3\)](#).

H₂ chemisorption results are given in [Table 1](#). Dispersion was calculated from H₂ chemisorption measurements as well. Pd/rGO and Pd/ENS250 were the catalysts that exhibited higher amounts of adsorbed H₂ per mass unit. In contrast, Pd/CNF showed the lowest uptake rate. On the other hand, low dispersion and large nanoparticle mean size was observed for the four catalysts, especially for Pd/CNF and Pd/AC. Metal nanoparticles with sizes below 2–2.5 nm do not have band structure typical of bulk metal and are electrodeficient [19]. Besides, H₂ preferentially adsorbs on high coordination sites [20], which could affect H₂ chemisorption results.

[Fig. 3](#) shows representative TEM images for the Pd-Cu/G, Pd-Cu/AC and Pd-Cu/ENS250 fresh catalyst and after 4 h of the NO₃⁻ reduction test. Frequency histograms, nanoparticle mean size and standard deviation are also shown. No significant differences in the nanoparticle mean size were observed between fresh and used catalysts. Pd-Cu/G showed a nanoparticle mean size of 3.4 nm with particle size up to 12 nm. Although good dispersion was observed, metal agglomerations up to 40 nm were identified. Pd-Cu/AC exhibited the lowest nanoparticle mean size (1.5 nm) and good metal dispersion, with particles not exceeding 3 nm throughout the sample studied. Pd-Cu/ENS250 showed the largest nanoparticle mean size of 3.6 nm.

According to EDX images shown in [Supplementary Material \(from Fig. S2 to S7\)](#), the metallic phase of the catalyst consists mainly of monometallic and bimetallic Pd and Cu nanoparticles, with different particle structures. Despite the good dispersion of both metal phases on the carbon supports, the images of the Pd-Cu/ENS250 and Pd-Cu/G catalysts suggest the existence of Pd nanoparticles on which the smaller Cu particles are deposited. Regarding the Pd-Cu/AC catalyst, there appear to be distinct zones where Pd is localized forming clusters, while Cu is dispersed throughout the support in particles of smaller size. Likewise, a minor contribution of nanoalloys was observed. On the other hand, no significant difference were observed between the images of the fresh and used catalyst.

XPS spectra were obtained to determine the oxidation state of Pd and Cu in the Pd-Cu fresh catalysts and after 4 h of reaction can be seen in [Supplementary Material \(Figs. S8 and S9\)](#), respectively. Binding energies that can be attributed to metallic Pd (Pd⁰) were in the range from 335.5 to 336.0 eV for Pd 3d_{5/2} and 340.8–341.5 eV for Pd 3d_{3/2}.

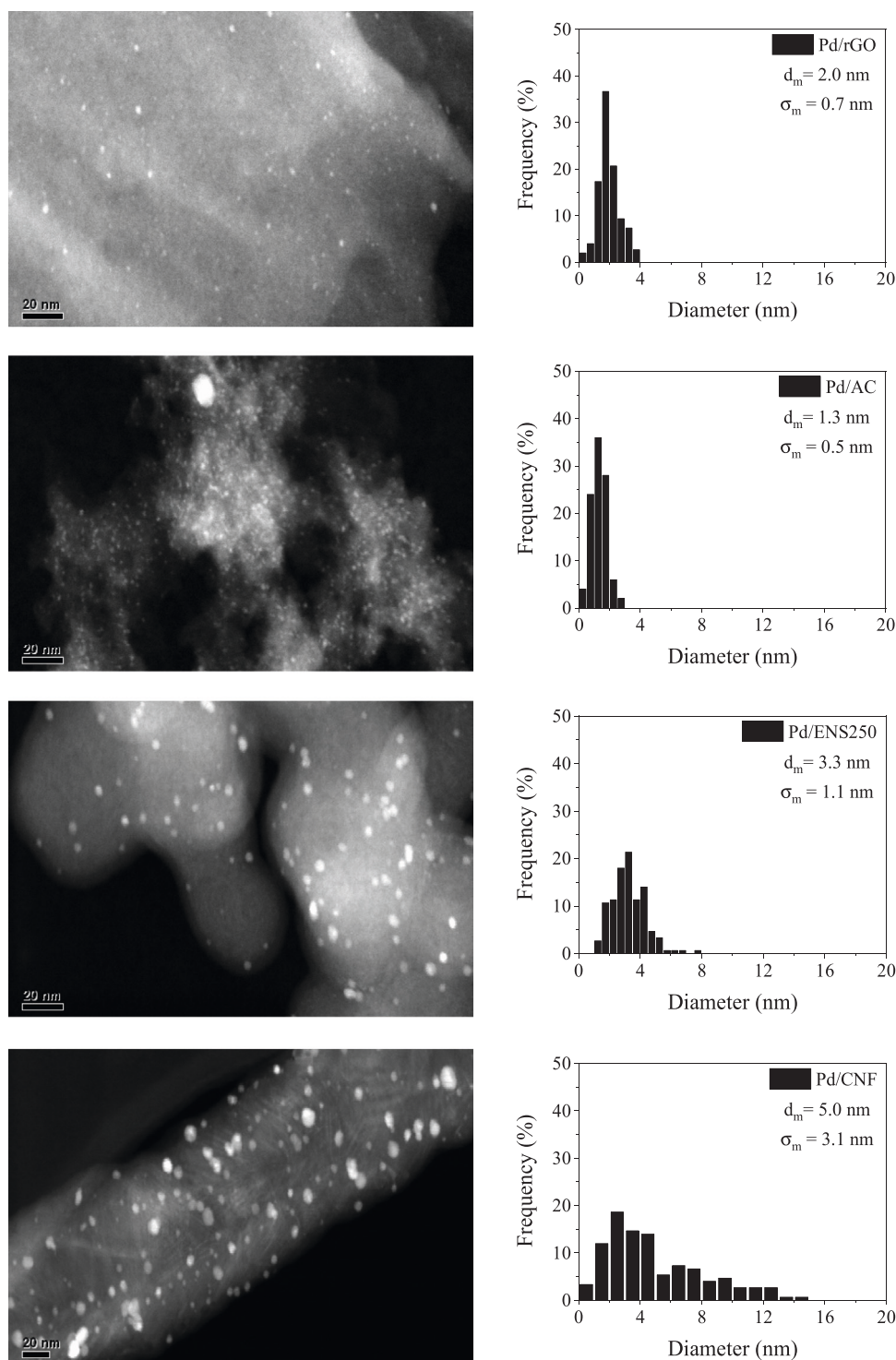


Fig. 2. TEM micrographs, nanoparticle size distributions, mean sizes and standard deviations for the Pd/C catalysts.

Table 1

H₂ chemisorption, metallic dispersion and nanoparticle mean size for the Pd catalysts tested.

Catalyst	H ₂ adsorbed (μmol/g)	Dispersion (%)
Pd/AC	7	2.9
Pd/rGO	12.1	5.1
Pd/ENS250	14.2	6.0
Pd/CNF	1.5	0.6

Electro-deficient Pd ($\text{Pd}^{\text{n}+}$) was attributed to the signal detected in the range from 336.9 to 337.7 eV for Pd 3d5/2 and 342.3–342.6 eV for Pd 3d3/2. Regarding metallic Cu (Cu^0), binding energies in the range from 933.6 to 934.2 eV were attributed to Cu 2p3/2, and from 953.7 to 954.0 eV were attributed to Cu 2p1/2. Electro-deficient Cu ($\text{Cu}^{\text{n}+}$) was detected in the range from 942.0 to 942.8 eV and 962.6–963.0 eV for Cu 2p3/2 and Cu 2p1/2, respectively. These data are in good agreement with data reported in NIST X-ray Photoelectron Spectroscopy Database [21]. In the case of Pd-Cu/AC, a proportion of Pd^0 as low as 11.0% was observed in the fresh catalyst, which increased to 31.2% in the used one

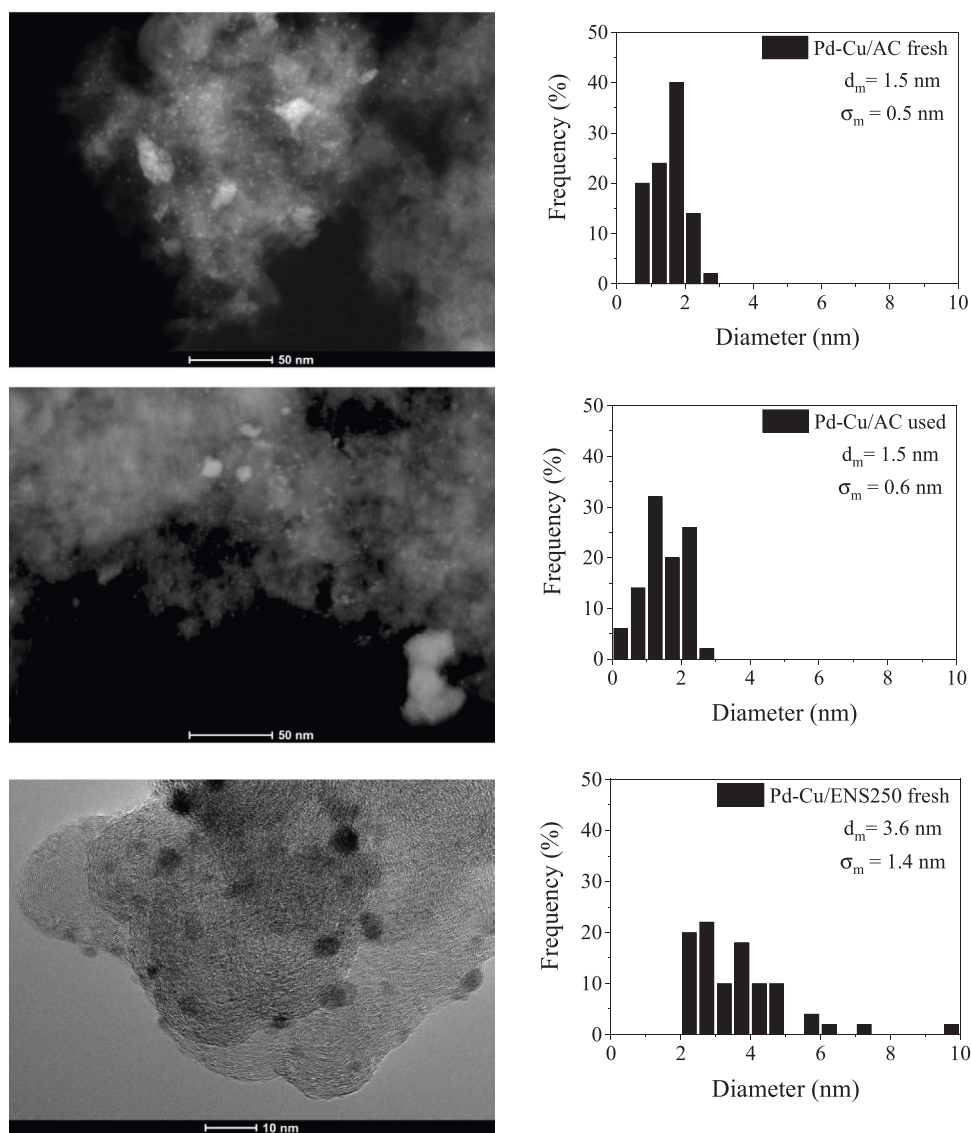


Fig. 3. TEM micrographs, nanoparticle size distributions, mean sizes and standard deviations for the Pd-Cu/G, Pd-Cu/AC and Pd-Cu/ENS250 fresh catalysts and after 4 h of reaction.

after 4 h of reaction. A significant increase in Pd^0 proportion was also observed for Pd-Cu/G after use, from 39.6% to 55.5%. Fresh Pd-Cu/ENS250 catalyst showed the highest percentage of Pd^0 (44.7%), which remained almost unchanged after NO_3^- reduction tests. Regarding Cu, the catalysts tested showed a similar Cu^0 proportion, around 70%, for the fresh catalyst, which decreased between 6.3% and 7.8% points when they were used.

3.2. Bromate, nitrite and nitrate reduction tests

Fig. 4 shows NO_2^- and BrO_3^- conversion vs reaction time curves for the Pd/C catalysts tested in a FTCMR equipped with 16 mm-diameter catalytic membranes. In the case of NO_2^- reduction (Fig. 4a), all the catalysts show conversion values between 80% and 98% in 4 h, Pd/ENS250 and Pd/AC being the most active catalysts. In the case of BrO_3^- reduction (Fig. 4b), the range of conversion was wider in the same reaction time, between 28% and 96%. Pd/rGO catalyst showed the lowest conversion in both NO_2^- and BrO_3^- reduction tests. Comparison of the results for FTCMR and batch or fixed-bed cannot be strictly performed, as the differences between experimental systems are significant. In that sense,

the FTCMR works in differential mode, and no direct contact between H_2 gas and catalyst active sites takes place. Likewise, only low H_2 or oxoanion gradients are expected to occur across the catalytic membrane. The comparison between NO_2^- and BrO_3^- reduction tests indicates that Pd/ENS250 and Pd/rGO catalysts show lower activity in the reduction of BrO_3^- than in the reduction of NO_2^- . These catalysts are characterized by a small nanoparticle mean size and narrow size distribution and have in common low conductivity of the support ($< 1 \text{ S/cm}$), according to Table S2. Moreover, Pd/CNF, which has the most conductive support (3.6 S/cm) but worse metallic dispersion, achieved conversion values from 90% for NO_2^- to 94% for BrO_3^- . In the case of Pd/AC, the great specific surface area may mask the role of the conductivity by the higher adsorption of compounds compared to the other supports tested. This suggests that the conductivity of the supports has a more important role in the case of BrO_3^- reduction, which may be related to charge distribution at the metal-carbon interface affecting the adsorption properties of Pd, and, thus, the catalytic activity [22]. Fig. 5 shows the selectivity to NH_4^+ vs NO_2^- conversion curves for NO_2^- reduction tests. Minor differences can be observed for the catalysts tested, with selectivity values lower than 2% at 80% conversion NO_2^- .

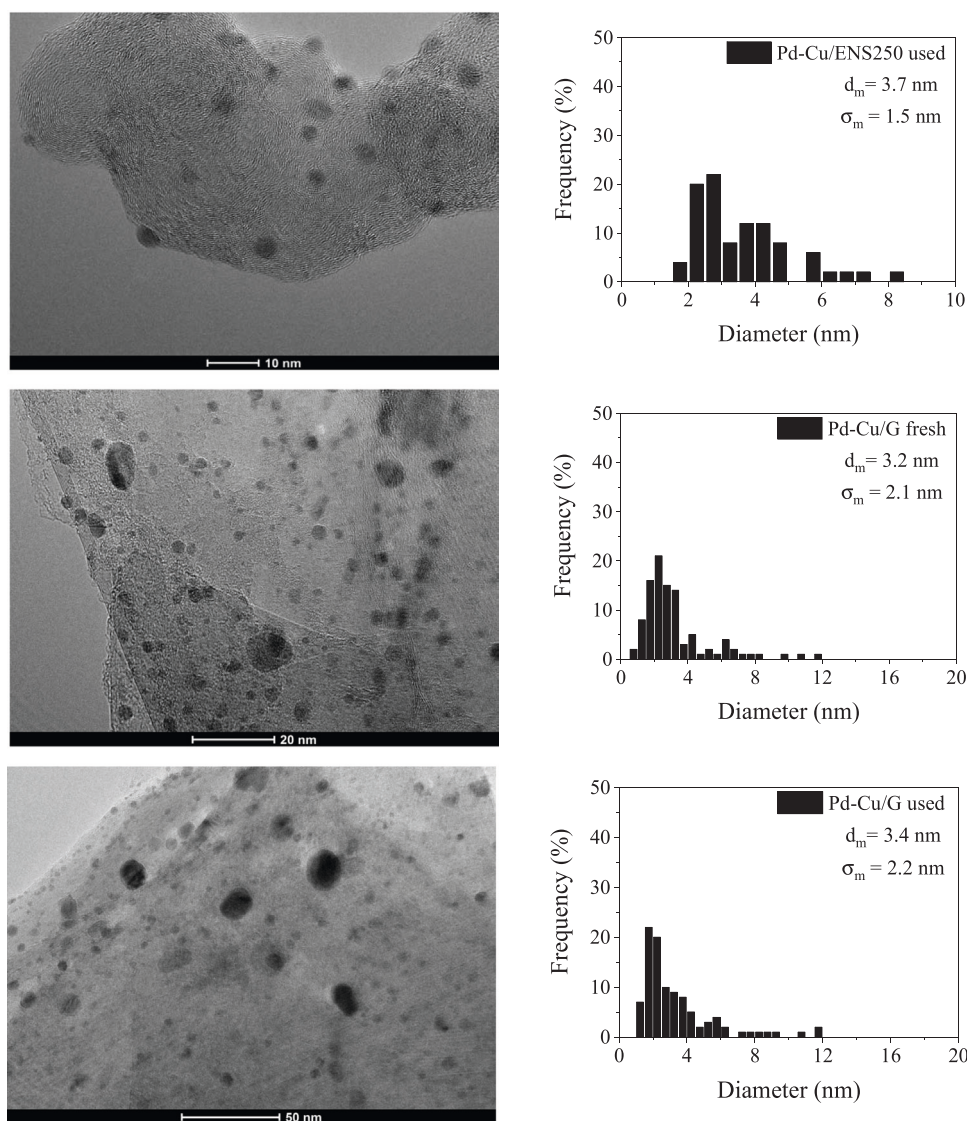


Fig. 3. (continued).

Previous to reduction tests, NO_3^- adsorption runs were conducted for 4 h in a slurry using 100 ppm of NO_3^- and 60 mg of catalyst in the absence of H_2 and CO_2 . The results obtained are shown in Table 2. In reduction essays, there is competition for the adsorption between other ions in addition to NO_3^- , such as HCO_3^- , NO_2^- and other N-intermediate species. Therefore, adsorption is expected to make a minority contribution to the conversion of NO_3^- . Furthermore, in a previous study, it was found that in the presence of H_2 , desorption of NO_3^- ions takes place due to competitive adsorption [23].

NO_3^- reduction tests were conducted using Pd-Cu catalysts in the FTCMR. Preliminary tests were performed using 16-mm diameter catalytic membranes, but the low conversion achieved for some catalysts (i. e., close to 10% for Pd-Cu/CNF) hindered the comparison of the catalytic performances. Thus, 30 mm-diameter catalytic membranes with higher catalyst load (60 mg) to increase NO_3^- conversion were prepared and tested. Fig. 6 shows NO_3^- conversion vs reaction time for the Pd-Cu catalysts tested in FTCMR. NO_3^- conversion was in a range from 23% to 100% in 4 h of reaction. Pd-Cu/AC and Pd-Cu/ENS250 were the most active catalysts, achieving complete conversion in 4 h of reaction. Pd-Cu/rGO was the less active catalyst among the used ones, and Pd-Cu/G, and Pd-Cu/CNF exhibited an intermediate behavior, with conversions in a range from 70% to 90% in 4 h of reaction. Pd-Cu/AC presents high specific surface area and small nanoparticle mean size (see Table S1

and S3) compared to Pd-Cu/ENS250, a catalyst with a relatively low surface area and larger nanoparticle mean size. No direct relationship between activity and specific surface area, nor mean nanoparticle size was found. Yoshinaga et al. [24] tested catalytic NO_3^- reduction in a fixed-bed reactor using Pd-Cu catalysts with different supports (activated carbon, silica, zirconia, and alumina), and they found that high specific surfaces areas of the supports were related to high active Pd-Cu catalysts. Other authors [25] could not find a clear relationship between activity and specific surface area in their experiments using Pd-Cu catalysts supported on different materials. In the case of the effect of nanoparticle size on catalyst activity, Papa et al. [26] reported that Pd-Cu catalysts supported on titania and alumina were more active when nanoparticle size was smaller, whereas other authors [27], reported higher activity in NO_3^- reduction when Pt/ SiO_2 catalysts with larger Pt metallic nanoparticles were used. Therefore, no conclusive trends are found in the literature regarding the influence of surface area and nanoparticle mean size in catalytic activity.

The selectivity to NH_4^+ vs NO_3^- conversion curves are shown in Fig. 7. The catalysts supported in Pd-Cu/ENS250 produced less NH_4^+ , showing NH_4^+ selectivity values close to 10%, followed by Pd-Cu/G and Pd-Cu/CNF, which exhibited selectivities around 35%, and Pd-Cu/AC with ca. 60% at 70% NO_3^- conversion. Pd-Cu/rGO showed high selectivity to NH_4^+ even at low conversion rates (45% at 25% NO_3^- conversion). Two of

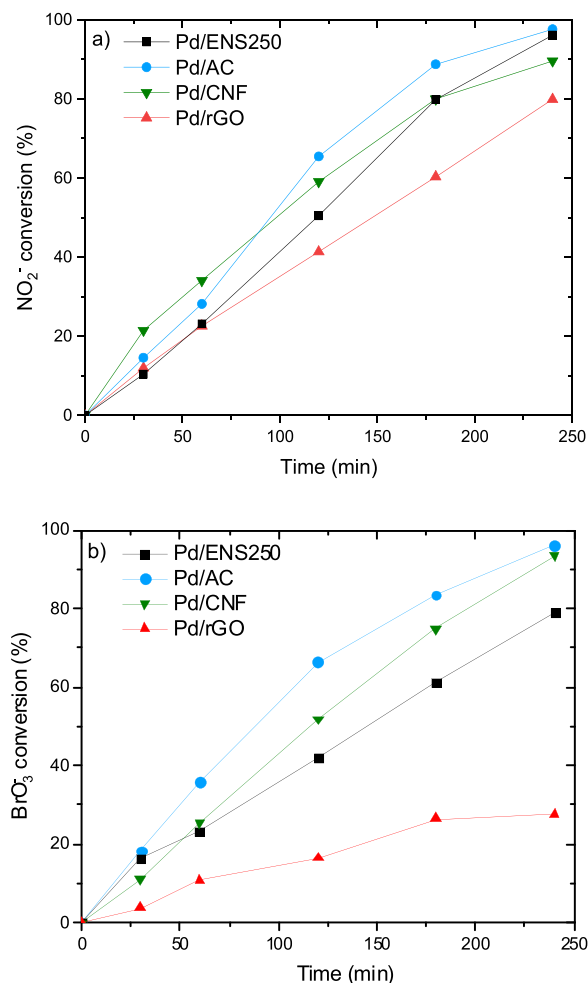


Fig. 4. (a) NO_2^- and (b) BrO_3^- conversion vs reaction time for the Pd /ENS250, Pd /AC, Pd /CNF, and Pd /rGO, catalysts in FTCMR ($[\text{NO}_2]_0 = [\text{BrO}_3]_0 = 30 \text{ mg/L}$, H_2 flow rate = $50 \text{ cm}^3 \text{ STP/min}$, CO_2 flow rate = $50 \text{ cm}^3 \text{ STP/min}$, 20 mg of catalyst, 16 mm in diameter FTCMR).

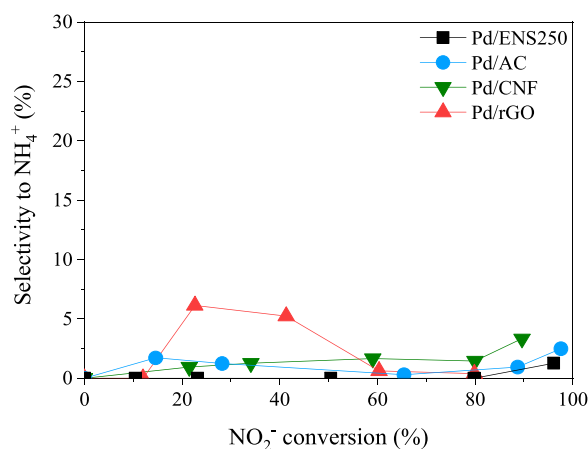


Fig. 5. Selectivity to NH_4^+ vs NO_2^- conversion for the Pd catalysts tested in FTCMR ($[\text{NO}_2]_0 = 30 \text{ mg/L}$, H_2 flow rate = $50 \text{ cm}^3 \text{ STP/min}$, CO_2 flow rate = $50 \text{ cm}^3 \text{ STP/min}$, 20 mg of catalyst, 16 mm in diameter FTCMR).

the catalysts yielding lower selectivity to NH_4^+ (Pd-Cu/G and Pd-Cu/ENS250) are characterized by nanoparticle sizes between 3 and 4 nm. Pd-Cu/ENS250, Pd-Cu/CNF, Pd-Cu/G, and Pd-Cu/AC, had 3.6, 6.5, 3.2, and 1.5 nm nanoparticle mean size, respectively, as shown in Fig. 3 and

Table 2

Adsorption rate of NO_3^- for the Pd-Cu catalysts tested.

Catalyst	mg NO_3^- ads/g catalysts	% of total NO_3^- adsorbed
Pd-Cu/G	3.82	6.4%
Pd-Cu/AC	7.68	12.8%
Pd-Cu/CNF	0.81	1.4%
Pd-Cu/rGO	0.83	1.4%
Pd-Cu/ENS250	4.06	6.8%

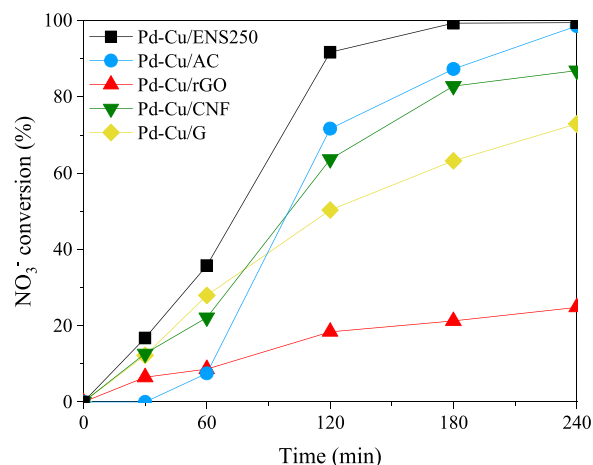


Fig. 6. NO_3^- conversion vs reaction time for the Pd-Cu catalysts tested in FTCMR ($[\text{NO}_3]_0 = 30 \text{ mg/L}$, H_2 flow rate = $50 \text{ cm}^3 \text{ STP/min}$, CO_2 flow rate = $50 \text{ cm}^3 \text{ STP/min}$, 60 mg of catalyst, 30 mm in diameter FTCMR).

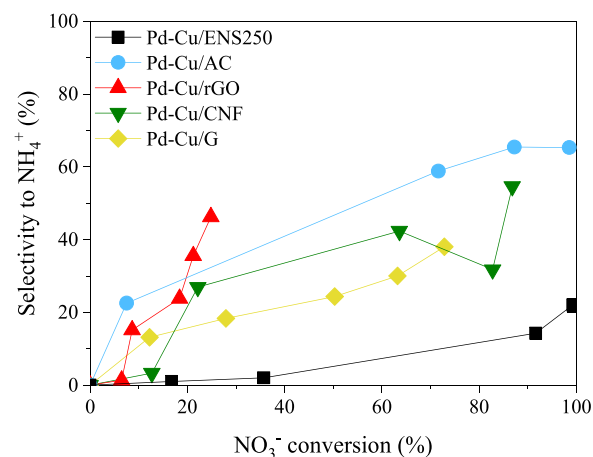


Fig. 7. Selectivity to NH_4^+ vs NO_3^- conversion for the Pd-Cu catalysts tested in FTCMR ($[\text{NO}_3]_0 = 30 \text{ mg/L}$, H_2 flow rate = $50 \text{ cm}^3 \text{ STP/min}$, CO_2 flow rate = $50 \text{ cm}^3 \text{ STP/min}$, 60 mg of catalyst, 30 mm in diameter FTCMR).

Table S3. According to the literature, large nanoparticle size reduces the production of NH_4^+ as less prevalence of low coordination atoms on the metallic surface, located at corners and edges, can be found [24,28]. Moreover, it has also been reported that catalysts with high electrical conductivity also reduce the selectivity to NH_4^+ , as they may enhance the charge transfer between metal and support [22]. Interestingly, Pd/rGO had a nanoparticle mean size of 3.8 nm and low electrical conductivity (0.8 S/cm). Pd-Cu/AC had the lower nanoparticle size (1.5 nm) and low electrical conductivity (0.4 S/cm) and it was prone to produce NH_4^+ .

Fig. 8 shows NO_3^- conversion vs reaction time and selectivity to NH_4^+ vs NO_3^- conversion for the Pd-Cu/G, Pd-Cu/AC and Pd-Cu/ENS250 catalysts at different H_2 flow rates in the saturation tank of the FTCMR. As CO_2 flow rate was maintained at $50 \text{ cm}^3 \text{ STP/min}$, decreasing the H_2

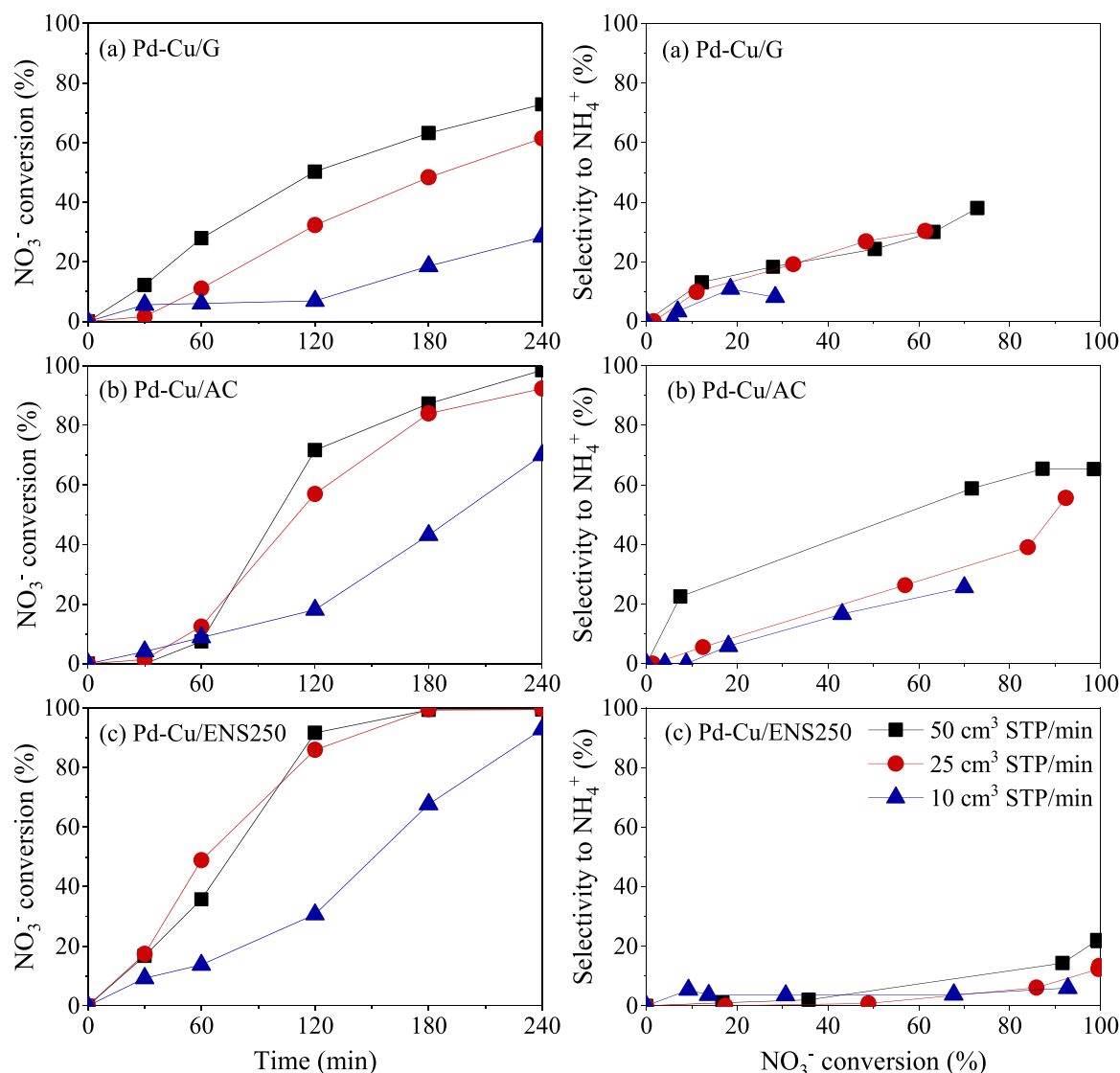


Fig. 8. NO_3^- conversion vs reaction time (left) and selectivity to NH_4^+ vs NO_3^- conversion (right) for the (a) Pd-Cu/G, (b) Pd-Cu/AC and (c) Pd-Cu/ENS250 catalysts in FTCMR at different H_2 flow rates: 50 cm^3 STP/min (0.78 mg/L), 25 cm^3 STP/min (0.52 mg/L) and 10 cm^3 STP/min (0.26 mg/L) - ($[\text{NO}_3^-]_0 = 30$ mg/L, CO_2 flow rate = 50 cm^3 STP/min, 60 mg of catalyst, 30 mm in diameter FTCMR).

flow rate from 50 cm^3 STP/min to 25 cm^3 STP/min and 10 cm^3 STP/min resulted in 0.78 mg/L, 0.52 mg/L and 0.26 mg/L of estimated H_2 solubilised, respectively. The lowest H_2 concentration in the reaction medium provoked a reduction in catalytic NO_3^- conversion for the three catalysts, especially when it was decreased from 0.52 mg/L to 0.26 mg/L. A reduction in selectivity to NH_4^+ was also observed in most cases, in agreement with the lower availability of H_2 . Interestingly, a decrease in H_2 concentration from 0.78 mg/L to 0.52 mg/L provoked a reduction in the selectivity to NH_4^+ of Pd-Cu/ENS250 and Pd-Cu/AC catalysts without a significant loss of NO_3^- conversion. In the case of Pd-Cu/G, NH_4^+ production was only slightly reduced when H_2 concentration decreased from 0.52 mg/L to 0.26 mg/L, but at the expense of NO_3^- conversion. Therefore, the reduction of H_2 concentration leads to lower H_2 availability and a reduction of H/N at the catalytic active sites, thus altering activity and selectivity to NH_4^+ . Although this behavior has been observed in all the three catalysts assayed, each one of them has performed in a different way, evidencing that both the H_2 availability, nanoparticle size and the catalysts support structure are relevant features.

3.2.1. Simultaneous reduction of nitrate, nitrite and bromate

Fig. 9 shows the simultaneous conversion of NO_3^- , NO_2^- and BrO_3^- vs reaction time for the Pd-Cu/G, Pd-Cu/rGO, Pd-Cu/AC and Pd-Cu/ENS250 catalysts in FTCMR with membranes 30 mm in diameter.

Complete conversion of BrO_3^- was observed for the four catalysts in 4 h of reaction. In the case of NO_2^- , total conversion was also achieved for Pd-Cu/rGO and Pd-Cu/AC, whereas Pd-Cu/G and Pd-Cu/ENS250 exhibited partial conversions of 30% and 90% in 4 h, respectively. Surprisingly, none of the catalysts was able to reduce NO_3^- , suggesting competitive reactions hindering NO_3^- or reaction products blocking active sites. The results obtained with Pd-Cu/G and Pd-Cu/ENS250 catalysts show that BrO_3^- is primarily converted at short reaction times, and that NO_2^- did not start to be significantly converted until ca. 50% of initial BrO_3^- was converted. This suggests competitive adsorption, although in the case of Pd-Cu/AC and Pd-Cu/rGO such effect was not so evident as NO_2^- was converted before BrO_3^- . Taking into account the nanoparticle size, which is significantly larger for Pd-Cu/G and Pd-Cu/ENS250 catalysts, competitive adsorption could take place preferentially in high coordination sites (i.e., terraces), more prevalent in larger nanoparticles, rather than low coordination sites (i.e., edges and corners).

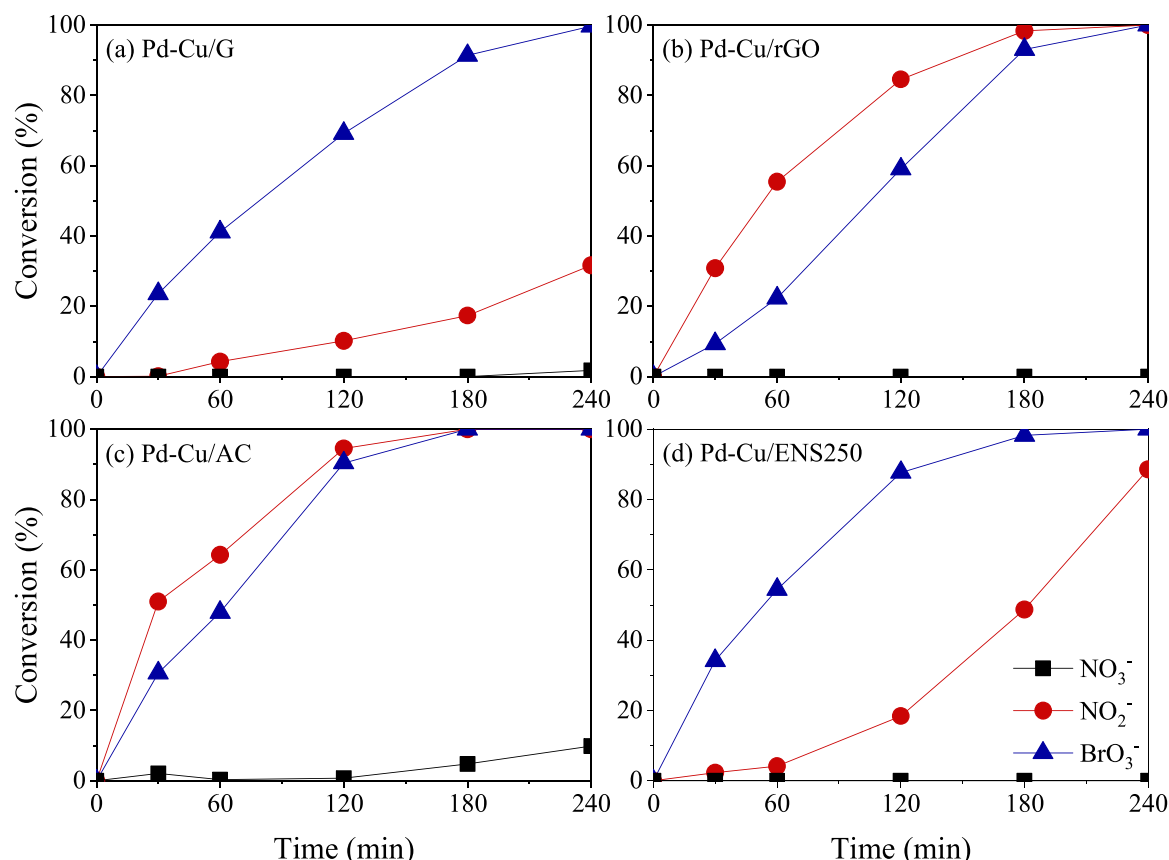


Fig. 9. NO_3^- , NO_2^- and BrO_3^- conversion vs reaction time for the (a) Pd-Cu/G, (b) Pd-Cu/rGO, (c) Pd-Cu/AC and (d) Pd-Cu/ENS250 catalysts in FTCMR ($[\text{NO}_3^-]_0 = [\text{BrO}_3^-]_0 = 20 \text{ mg/L}$, $[\text{NO}_2^-]_0 = 10 \text{ mg/L}$, H_2 flow rate = $50 \text{ cm}^3 \text{ STP/min}$, CO_2 flow rate = $50 \text{ cm}^3 \text{ STP/min}$, 60 mg of catalyst, 30 mm in diameter FTCMR).

Fig. 10 depicts the selectivity to NH_4^+ vs NO_2^- conversion for the Pd-Cu/G, Pd-Cu/rGO, Pd-Cu/AC and Pd-Cu/ENS250 catalysts in FTCMR. All the catalysts exhibited low NH_4^+ production, being the Pd-Cu/ENS250 catalyst the one with the highest selectivity (around 15%). In all the cases, selectivity to NH_4^+ vs NO_2^- conversion plot showed a volcano shape. This could partially be explained by the competitive adsorption in high coordination sites where BrO_3^- prevails over NO_2^- , favouring the adsorption of NO_2^- at early reaction time in low coordination sites, responsible for the overreduction of the adsorbed N-

intermediated species.

With the aim of deepening the role of Br species in the catalyst behavior, a test in which both NO_3^- and Br^- were introduced at the same time in the reactor at $t = 0$ was performed. Fig. 11 shows the NO_3^- and Br^- disappearance vs time, the first ascribed to reduction and the second ascribable to adsorption. Both NO_3^- and Br^- disappearance was low (approx. 4% and 6%, respectively), suggesting that Br^- inhibits Pd-Cu/ENS250 ability to reduce NO_3^- . However, as shown in Fig. 9, the ability to reduce NO_2^- by Pd-Cu/ENS250 in the presence of Br species was not

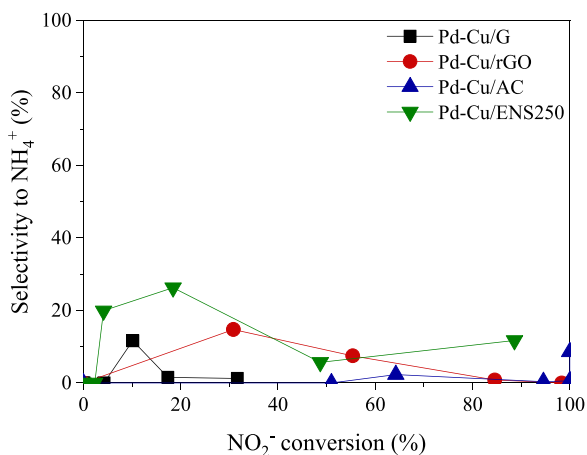


Fig. 10. Selectivity to NH_4^+ vs NO_2^- conversion for the Pd-Cu catalysts tested in FTCMR ($[\text{NO}_3^-]_0 = [\text{BrO}_3^-]_0 = 20 \text{ mg/L}$, $[\text{NO}_2^-]_0 = 10 \text{ mg/L}$, H_2 flow rate = $50 \text{ cm}^3 \text{ STP/min}$, CO_2 flow = $50 \text{ cm}^3 \text{ STP/min}$, 60 mg of catalyst, 30 mm in diameter FTCMR).

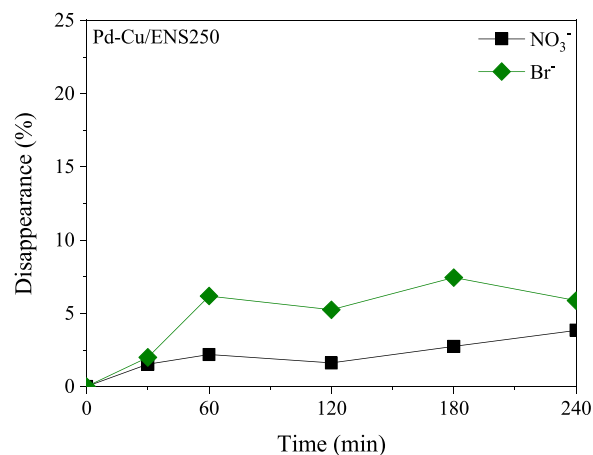


Fig. 11. NO_3^- conversion vs reaction time in the presence of Br^- for the Pd-Cu/ENS250 catalysts in FTCMR ($[\text{NO}_3^-]_0 = [\text{Br}^-]_0 = 20 \text{ mg/L}$, H_2 flow rate = $50 \text{ cm}^3 \text{ STP/min}$, CO_2 flow rate = $50 \text{ cm}^3 \text{ STP/min}$, 60 mg of catalyst, 30 mm in diameter FTCMR).

significantly affected, indicating that the poisoning mechanism could be hindering the Pd-Cu redox cycle, which is crucial for the first steps in catalytic NO_3^- reduction [29,30]. Moreover, whereas the role of Cl species poisoning Pd catalysts in hydrogenation/hydrogenolysis reactions is well established [31], reports on Br species poisoning metal catalysts are very scarce. However, detrimental Br⁻ effect in catalysts activity can be attributed to inhibition following similar mechanisms as Cl⁻ since they have a similar electronic structure. Some studies have reported the inhibitory effect of Cl⁻ in NO_3^- catalytic reduction and an increase in selectivity to NH_4^+ in concentrations up to 200 mg/L when Pd-Cu/ $\gamma\text{-Al}_2\text{O}_3$ and Pd-Cu/AC catalysts were used [32,33]. This behavior has been ascribed to the preferential adsorption of Cl⁻ over NO_3^- on the Cu active sites and the accumulation of Cl⁻ on the Helmholtz layer, leading to the deprotonation of the catalyst surface increasing the repulsion of NO_3^- ions [34]. Furthermore, studies on the influence of HBr in tar reforming using Ni-based catalysts have shown that Br can be chemisorbed on Ni surface, decreasing the number of active sites in higher extension compared to Cl [35].

It is worthy to note that the field of application of catalytic reduction is drinking water, where Br⁻ pollution is not expected to occur at concentrations similar to those characteristic of Cl⁻. However, the results show that cumulative exposure of catalysts to Br⁻ can result in the deactivation of the catalysts, which could condition the order of the disinfection step, in which Br species can be formed.

4. Conclusions

Pd- and Pd-Cu-based catalytic membranes prepared from powder catalysts and tested in FTCMR have shown to be active in the reduction of NO_3^- , NO_2^- and BrO_3^- , suggesting their potential for practical applications. In the case of Pd-based catalytic membranes, the conductivity of the support seems to have a more important role in the case of BrO_3^- reduction, which could be related to the charge distribution at the metal-carbon interface and its effect on the adsorption properties of Pd, affecting activity. Selectivity to NH_4^+ was low in all the NO_2^- reduction experiments, being < 2% at 80% of NO_2^- conversion.

Pd-Cu-based catalytic membranes were also active in the reduction of NO_3^- . Moreover, catalytic membranes based on the catalyst with large nanoparticle mean size and high support conductivity exhibited lower NH_4^+ content in the treated water. This behavior may be due to the low prevalence of low coordination sites that favor the overreduction of N-species adsorbed on catalysts surface, and the improved charge transfer at the metal-carbon interface in supports with high conductivity, limiting NH_4^+ production.

FTCMR configuration allowed to check the catalysts behavior at different H_2 availabilities in the reaction medium, favouring the search for optimized operation conditions to maintain low or decreasing the selectivity to NH_4^+ without (or with small) affection to activity. NO_3^- reduction is inhibited in the presence of Br species and could affect the Pd-Cu redox cycle. This is a remarkable fact since it clearly conditions the order of the disinfection and nitrate reduction steps in drinking water purification processes.

CRedit authorship contribution statement

A. Marí: Investigation, Writing – original draft, formal analysis. **J.A. Baeza:** Investigation, Formal analysis, Writing – review & editing. **M. Pedrosa:** Investigation, Formal analysis. **O. Salome G.P. Soares:** Conceptualization, Validation, Funding acquisition. **L. Calvo:** Conceptualization, Validation, Funding acquisition. **M.A. Gilarranz:** Supervision, Funding acquisition. **Adrian M. T. Silva:** Supervision, Funding acquisition. **M. Fernando R. Pereira:** Supervision, Funding acquisition.

Declaration of Competing Interest

The authors declare that they have no known competing financial

interests or personal relationships that could have appeared to influence the work reported in this paper.

Data availability

Data will be made available on request.

Acknowledgments

The authors greatly appreciate the support from Spanish Agencia Estatal de Investigación (AEI, RTI2018-098431-BI00). Adrián Marí thanks the Spanish AEI for a research grant (PRE-2019-088601). This work was also financially supported by: LA/P/0045/2020 (ALICE), UIDB/50020/2020 and UIDP/50020/2020 (LSRE-LCM) and funded by national funds through FCT/MCTES (PIDDAC), and project NORTE-01-0145-FEDER-000069 (Healthy Waters) co-funded by European Regional Development Fund (ERDF), through North Portugal Regional Operational Program (NORTE2020), under the PORTUGAL 2020 Partnership Agreement.

Appendix A. Supporting information

Supplementary data associated with this article can be found in the online version at doi:10.1016/j.jece.2023.109772.

References

- [1] K. Su, L. Li, S. Deng, Z. Gao, Q. Qin, J. Yang, S. Zhang, J. Chen, Research progress of TiO_2 photocatalytic reduction of oxyanion pollutants in water: a mini review, *Green Chem. Lett. Rev.* 15 (2022) 35–44.
- [2] X. Zhao, G. Zhang, Z. Zhang, TiO_2 -based catalysts for photocatalytic reduction of aqueous oxyanions: state-of-the-art and future prospects, *Environ. Int.* 136 (2020), 105453.
- [3] G. Mendow, C.I. Grosso, A. Sánchez, C.A. Querini, Hybrid process for the purification of water contaminated with nitrites: ion exchange plus catalytic reduction, *Chem. Eng. Res. Des.* 125 (2017) 348–360.
- [4] DIRECTIVE (EU) 2020/2184 OF THE EUROPEAN PARLIAMENT AND OF THE COUNCIL of 16 December 2020 on the quality of water intended for human consumption, ANNEX I: PARAMETERS AND PARAMETRIC VALUES, PART B: Chemical parameters.
- [5] H.O. World, Nitrate and nitrite in drinking-water: background document for development of WHO guidelines for drinking-water quality (2003).
- [6] S. Sharma, B.G. Pollet, Support materials for PEMFC and DMFC electrocatalysts-a review, *J. Power Sources* 208 (2012) 96–119.
- [7] P. Kumari, N. Bahadur, L.F. Dumée, Photo-catalytic membrane reactors for the remediation of persistent organic pollutants - a review, *Sep. Purif. Technol.* 230 (2020), 115878.
- [8] N. Li, X. Lu, M. He, X. Duan, B. Yan, G. Chen, S. Wang, Catalytic membrane-based oxidation-filtration systems for organic wastewater purification: a review, *J. Hazard. Mater.* 414 (2021), 125478.
- [9] J. Sheng, H. Yin, F. Qian, H. Huang, S. Gao, J. Wang, Reduced graphene oxide-based composite membranes for in-situ catalytic oxidation of sulfamethoxazole operated in membrane filtration, *Sep. Purif. Technol.* 236 (2020), 116275.
- [10] C. Chen, M. Xie, L. Kong, W. Lu, Z. Feng, J. Zhan, Mn_3O_4 nanodots loaded g-C $_3\text{N}_4$ nanosheets for catalytic membrane degradation of organic contaminants, *J. Hazard. Mater.* 390 (2020), 122146.
- [11] T. Qiu, J. Yang, X. Bai, Y. Wang, The preparation of synthetic graphite materials with hierarchical pores from lignite by one-step impregnation and their characterization as dye adsorbents, *RSC Adv.* 9 (2019) 12737–12746.
- [12] A. Marí, J.A. Baeza, L. Calvo, M.A. Gilarranz, Catalytic membrane reactor based on Pd-Sn supported on nanocarbons for the reduction of nitrate in water, *J. Environ. Chem. Eng.* 10 (2022), 108011.
- [13] M. Pedrosa, G. Drazic, P.B. Tavares, J.L. Figueiredo, A.M.T. Silva, Metal-free graphene-based catalytic membrane for degradation of organic contaminants by persulfate activation, *Chem. Eng. J.* 369 (2019) 223–232.
- [14] A. Schmidt, R. Haidar, R. Schomäcker, Selectivity of partial hydrogenation reactions performed in a pore-through-flow catalytic membrane reactor, *Catal. Today* 104 (2005) 305–312.
- [15] T. Westermann, T. Melin, Flow-through catalytic membrane reactors-principles and applications, *Chem. Eng. Process. Process. Intensif.* 48 (2009) 17–28.
- [16] O.M. Ilinitch, F.P. Cuperus, L.V. Nosova, E.N. Gribov, Catalytic membrane in reduction of aqueous nitrates: operational principles and catalytic performance, *Catal. Today* 56 (2000) 137–145.
- [17] O.M. Ilinitch, E.N. Gribov, P.A. Simonov, Water denitrification over catalytic membranes: hydrogen spillover and catalytic activity of macroporous membranes loaded with Pd and Cu, *Catal. Today* 82 (2003) 49–56.
- [18] D.T. González, A. Marí, J.A. Baeza, L. Calvo, M.A. Gilarranz, Enhancement of activity and selectivity to nitrogen in catalytic nitrate reduction by use of

- conductive carbon catalytic supports and control of hydrogen mass transfer regime, *J. Environ. Chem. Eng.* 9 (2021), 106419.
- [19] A.Y. Stakheev, I.S. Mashkovskii, G.N. Baeva, N.S. Telegina, Specific features of the catalytic behavior of supported palladium nanoparticles in heterogeneous catalytic reactions, *Russ. J. Gen. Chem.* 80 (2010) 618–629.
- [20] W. Dong, V. Ledentu, P. Sautet, A. Eichler, J. Hafner, Hydrogen adsorption on palladium: a comparative theoretical study of different surfaces, *Surf. Sci.* 411 (1998) 123–136.
- [21] NIST X-ray Photoelectron Spectroscopy Database. <http://srdata.nist.gov/xps/> (Retrieved on February 2, 2023).
- [22] R.G. Rao, R. Blume, T.W. Hansen, E. Fuentes, K. Dreyer, S. Moldovan, O. Ersen, D. D. Hibbitts, Y.J. Chabal, R. Schlögl, J. Tessonnier, Interfacial charge distributions in carbon-supported palladium catalysts, *Nat. Commun.* 8 (2017) 340.
- [23] A.M. Pérez-Coronado, L. Calvo, J.A. Baeza, J.J. Rodriguez, M.A. Gilarranz, Control of selectivity in the reduction of nitrate by shielding of Pd-Cu/C catalysts with AOT, *J. Ind. Eng. Chem.* 82 (2020) 42–49.
- [24] Y. Yoshinaga, T. Akita, I. Mikami, T. Okuhara, Hydrogenation of nitrate in water to nitrogen over pd-cu supported on active carbon, *J. Catal.* 207 (2002) 37–45.
- [25] O.S.G.P. Soares, J.J.M. Órfão, M.F.R. Pereira, Nitrate reduction in water catalysed by Pd-Cu on different supports, *Desalination* 279 (2011) 367–374.
- [26] F. Papa, I. Balint, C. Negri, E. Olaru, I. Zgura, C. Bradu, Supported Pd-Cu nanoparticles for water phase reduction of nitrates. influence of the support and of the ph conditions, *Ind. Eng. Chem. Res.* 53 (2014) 19094–19103.
- [27] K. Shafqat, S. Pitkääho, M. Tiainen, L. Matějová, R.L. Keiski, Effect of nanoparticle size in pt/sio2 catalyzed nitrate reduction in liquid phase, *Nanomaterials* 11 (2021).
- [28] J.K. Chinthaginjala, L. Lefferts, Support effect on selectivity of nitrite reduction in water, *Appl. Catal. B Environ.* 101 (2010) 144–149.
- [29] F. Epron, F. Gauthard, C. Pinéda, J. Barbier, Catalytic reduction of nitrate and nitrite on pt-cu/al₂o₃ catalysts in aqueous solution: role of the interaction between copper and platinum in the reaction, *J. Catal.* 198 (2001) 309–318.
- [30] J. Martínez, A. Ortiz, I. Ortiz, State-of-the-art and perspectives of the catalytic and electrocatalytic reduction of aqueous nitrates, *Appl. Catal. B Environ.* 207 (2017) 42–59.
- [31] V.R. Choudhary, M.G. Sane, Poisoning of Pd-carbon catalysts by sulphur chloro and heavy metal compounds in liquid phase hydrogenation of o-nitrophenol to o-aminophenol, *J. Chem. Technol. Biotechnol.* 73 (1998) 336–340.
- [32] B.P. Chaplin, E. Roundy, K.A. Guy, J.R. Shapley, C.J. Werth, Effects of natural water ions and humic acid on catalytic nitrate reduction kinetics using an alumina supported pd⁰/cu catalyst, *Environ. Sci. Technol.* 40 (2006) 3075–3081.
- [33] Y. Wang, Y. Sakamoto, Y. Kamiya, Remediation of actual groundwater polluted with nitrate by the catalytic reduction over copper-palladium supported on active carbon, *Appl. Catal. A Gen.* 361 (2009) 123–129.
- [34] A. Pintar, J. Batista, I. Mušević, Palladium-copper and palladium-tin catalysts in the liquid phase nitrate hydrogenation in a batch-recycle reactor, *Appl. Catal. B Environ.* 52 (2004) 49–60.
- [35] D.K. Binte Mohamed, A. Veksha, T. Lim, G. Lisak, Hydrogen bromide in syngas: effects on tar reforming water gas-shift activities and sintering of Ni-based catalysts, *Appl. Catal. B Environ.* 280 (2021), 119435.